J Solid State Electrochem (2009) 13:967–973
DOI 10.1007/s10008-008-0631-2

ORIGINAL PAPER

Electrodeposition of platinum–nickel alloy nanocomposites on polyaniline-multiwalled carbon nanotubes for carbon monoxide redox

Guan-Ping Jin · Xia Peng · Yan-Feng Ding · Wan-Qing Liu · Jian-Ming Ye

Received: 19 June 2008 / Revised: 16 July 2008 / Accepted: 16 July 2008 / Published online: 14 August 2008

Abstract An electrochemical method was developed to deposit platinum (Pt)–nickel (Ni) alloy nanocomposites on polyaniline-multiwalled carbon nanotubes (Pt–Ni/PAN/MWCNTs). The material was characterized by various methods including field emission scanning electron microscope, X-ray diffraction, X-ray photoelectron spectroscopy, and electrochemical techniques. An appreciably improved catalysis toward oxidation of carbon monoxide (CO) was observed at the Pt–Ni/PAN/MWCNTs nanocomposites (real ratio of Pt–Ni of 17:1), which was interpreted by a mechanism based on the bifunctional catalysis. The successful preparation of Pt–Ni/PAN/MWCNTs nanocomposites opens a new path to synthesize the promising catalysts for CO.

Keywords Electrodeposition · Platinum–nickel nanocomposites · Multiwalled carbon nanotubes · Carbon monoxide

G.-P. Jin · X. Peng · Y.-F. Ding
Anhui Key Laboratory of Controllable Chemistry Reaction and Material Chemical Engineering, School of Chemical Engineering, Hefei University of Technology, Hefei 230009, People's Republic of China

G.-P. Jin (✉) · X. Peng · Y.-F. Ding
Department of Application Chemistry of School of Chemical Engineering, Hefei University of Technology, Hefei 230009, People's Republic of China
e-mail: jgp@hfut.edu.cn

W.-Q. Liu · J.-M. Ye
Hefei Huaqing Metal Surfacing Co., Ltd, Hefei 230009, People's Republic of China

Introduction

Carbon monoxide, a dangerous toxic gas, can cause serious health hazards, when combined with the hemoglobin and stopping transporting oxygen in body, and can also poison platinum catalysts in fuel cell by adsorbing at active site [1]. More significantly, both portable monitoring for CO and avoidance for platinum catalysts poisoning have motivated researchers worldwide. For the former one, electrochemical sensors [2, 3] have many advantages over other types [4, 5] in terms of linear output, low power requirement, and economy. One of the major approaches is the effective utilization of metal nanoparticles due to their high surface area and device miniaturization [2, 6–10]. For the latter one, Pt–Ni bimetallic catalyst has attracted an increasing interests [1, 11–17], which can appreciably improve the resistance to CO poisoning, the oxidation of methanol, and the reduction of oxygen and carbon dioxide [13, 14, 16, 17], and can also decrease oxidation potential of CO [10].

The application of multiwalled carbon nanotubes (MWCNTs) for gas sensors has received great attraction because of fast response, good sensitivity, and low operating temperature [18–21]. Theoretical studies have confirmed the remarkable change in electronic properties and gas detection [18, 22]. MWCNTs also have been regarded as a new support for metal catalysts due to their small size, high chemical–thermal–mechanical stabilities, and large surface area [23–26]. Nevertheless, only a few studies for Pt–Ni/MWCNTs preparation were reported. Yen et al. reported a green method using supercritical fluid carbon dioxide as soluble metal precursors [16]. Zhao et al. introduced a new route using three-step electrodeposition process for the direct methanol fuel cells [1]. In comparison with the two kinds of methods, the latter method may be

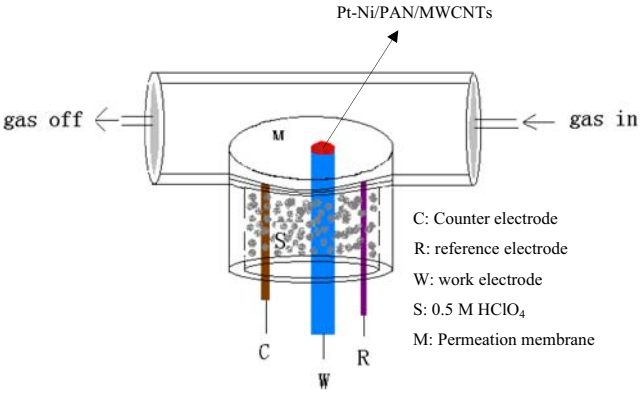

Fig. 1 The scheme of CO sensor

advantageous in terms of high purity, simple procedure, and economy. However, electrodeposition of Pt and Ni nanocomposites on MWCNTs has not been achieved so far. In this work, we suggest a simple approach for electrodeposition of platinum–nickel alloy nanocomposites on polyaniline-multiwalled carbon nanotubes through molecular level design (Pt–Ni/PAN/MWCNTs); the effect of the catalysts was investigated toward the redox of CO.

Experiment section

Reagents and equipment

MWCNTs with diameters of 10–30 nm and lengths of 1–10 μm were purchased from Sun Nanotech. Co. Ltd. of China and were synthesized by catalytic decomposition of CH_4 on a NiMgO catalyst [23]. Aniline, nickel (II) sulfate ($NiSO_4$, 99.9%) and potassium tetrachloroplatinate (II) (Cl_4K_2Pt) were purchased from Chemical Reagent Company of Shanghai (China). Carbon monoxide (CO, 99.99%) was supplied by Shang Yuan Gas Company of Najing (Najing, China). Nafion was purchased from Aldrich (Poole, UK). All the reagents were used without further purification. All solutions and subsequent dilutions were prepared using purified water (prepared in a quartz apparatus). High purity nitrogen gas was used for deaeration.

Electrochemical measurements were performed with a model CHI 660 B electrochemical analyzer (Cheng-Hua, Shanghai, China). A paraffin-impregnated graphite electrode (WGE) with geometric area of 0.125 cm^{-2} was used as working electrode [23]. A saturated calomel electrode (KCl) or Ag–AgCl was used as the reference electrode, and a platinum wire was used as the auxiliary electrode. Field emission scanning electron microscope (FE-SEM) images were obtained on a JSM-600 field emission scanning electron microanalyzer (JEOL, Japan). X-ray photoelectron spectra were recorded by using an $ESCALABMK_2$ spectrometer (Vg Corporation, UK) with Mg-Alpha X-ray radiation as the source for excitation. X-ray diffraction (XRD) data of the samples were collected using a Rigaku D/MAX-rB diffractometer with Cu Kαradiation.

Preparation of Pt–Ni/PAN/MWCNTs/WGE

The 10-mg MWCNTs were dispersed in 10 ml of mixed acid solution of nitric acid and perchlorate acid (7:3). The mixed solution was ultrasonically agitated for 7 h. The MWCNTs were washed with doubly distilled water to a neutral pH then washed with acetone and dried in air. The peaks at 1,735 and 1,590 cm^{-1} in the Fourier transform infrared spectrum suggested that carboxylic acid groups and carboxylate groups were present on the surface of the MWCNTs [23]. About 2.5 mg of mixed acid-treated MWCNTs was dispersed in 10 ml of acetone and 0.5 wt. % nafion with the aid of ultrasonic agitation to give 0.25-mg ml^{-1} black suspension.

The WGE was polished step-by-step to a mirror-like finish with fine wet emery paper (grain size 1,000, 3,000, and 4,000), followed by sonication in ethanol and water for 15 min, respectively. After cleaning, 30 μL of the suspension was directly cast on WGE surface and evaporated in the solvent at room temperature (MWCNTs/WGE).

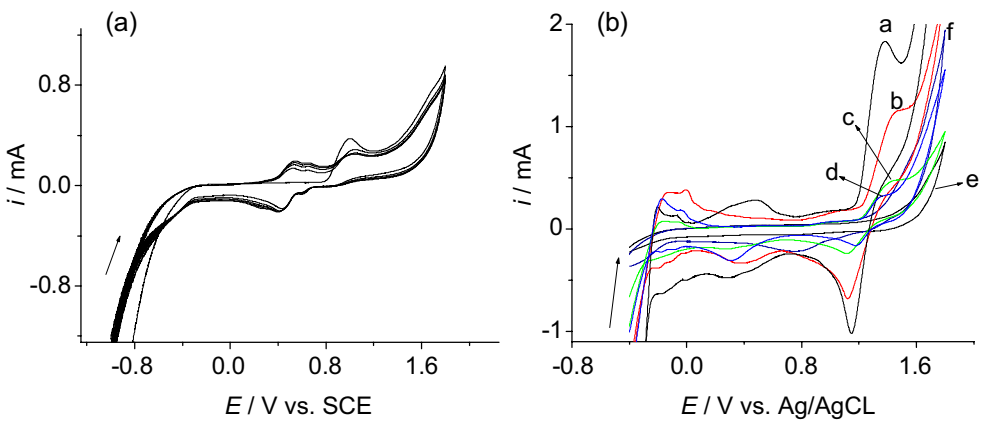

Fig. 2 **a** CVs of MWCNTs/WGE in 0.01 M aniline in 0.5 M H_2SO_4. **b** CVs of bare WGE (*e*), Ni/PAN/MWCNTs/WGE (*f*), Pt/PAN/MWCNTs/WGE (*a*), solution concentration ratio of Pt–Ni=1:1 (*b*), or 1:3 (*c*), or 1:6 (*d*) /PAN/MWCNTs/WGE in 0.5 M $HClO_4$. Potential range: −1.0–1.8 V. Scan: 50 mV s^{-1}

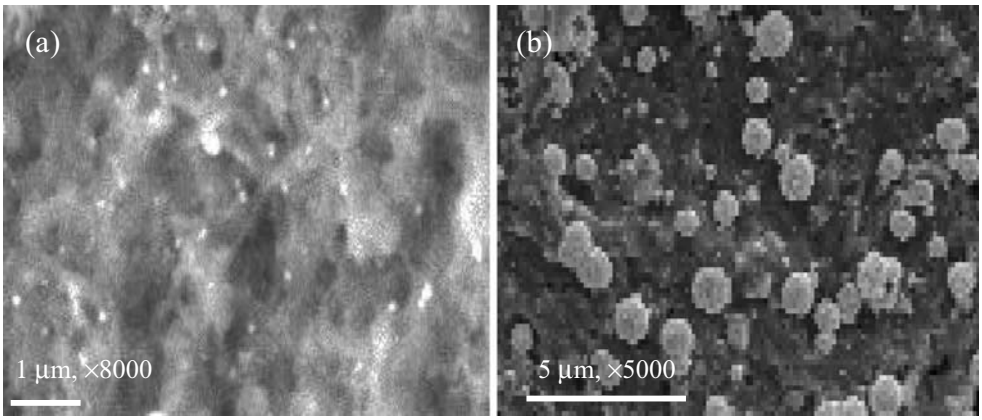

Fig. 3 **a** FE-SEM of Pt–Ni/PAN/MWCNTs using constant potential and CV step. **b** FE-SEM of Pt–Ni/PAN/MWCNTs using direct CV method. Pt–Ni solution concentration ratio, 1:1

The electrosynthesis of Pt–Ni/PAN/MWCNTs was used following two steps: PAN/MWCNTs/WGE was formed using cyclic voltammetry (CV) method in 0.01 M aniline + 0.5 M H_2SO_4. After rinsing with distilled water, the PAN/MWCNTs/WGE was transferred into an aqueous solution containing 0.1 mM Cl_4K_2Pt–0.1 mM $NiSO_4$ (or 0.3 or 0.6 mM)–0.1 M H_2SO_4 by a constant potential step at −0.3 V with 400 s to form $-NH-PtCl_4^{2-}$ and $-NH-Ni^{2+}$ complex; then, the complexes were transferred to form platinum–nickel alloy nanocomposites by successively potential cycling from −0.4 to 1.8 V with 25 cycles in 0.1 M H_2SO_4. The electrode was employed as the working electrode in CO electroanalysis (Pt–Ni/PAN/MWCNTs/WGE).

Preparation of the CO gas sensor

Figure 1 shows the structure of the CO gas sensor, which is similar to the structure of the traditional Clark-type gas sensor [27]. It had Pt–Ni/PAN/MWCNTs/WGE as working electrode, Ag–AgCl electrode as reference electrode, Pt wire as counter electrode, and selective permeable porous film (polyethylene) in contact with the gas-containing atmosphere.

Results and discussion

Electrochemical preparation of platinum–nickel nanocomposites on MWCNTs

Figure 2a shows the electrochemistry of polyaniline of aniline on the multiwalled carbon nanotubes surface at WGE in 0.01 M aniline–0.5 M H_2SO_4 (PAN/MWCNTs/WGE). There is only one pair of peak for the first cycle, and on the subsequent cycling, there are three pairs of peaks. The two sets of peaks located at 0.55–0.42 and 1.10–0.92 V corresponding to leucoemeraldine–emeraldine and emeraldine–pernigraniline transformations, respectively, and the third pair of peaks in the middle are attributed to

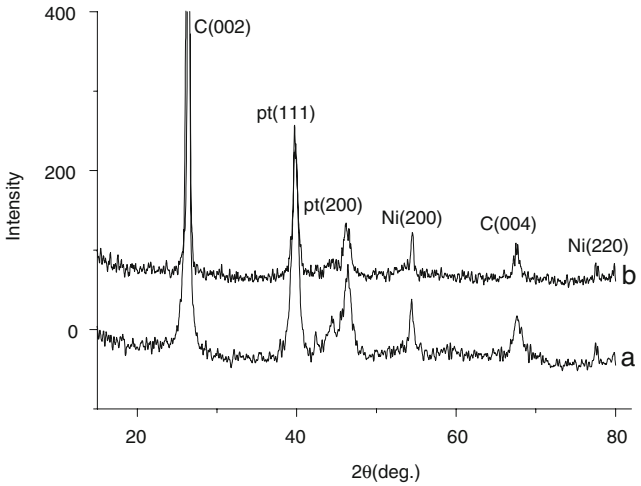

Fig. 4 XRD of Pt–Ni/PAN/MWCNTs obtained by constant potential and CV step (*a*) or direct CV step (*b*). Pt–Ni solution concentration ratio, 1:1

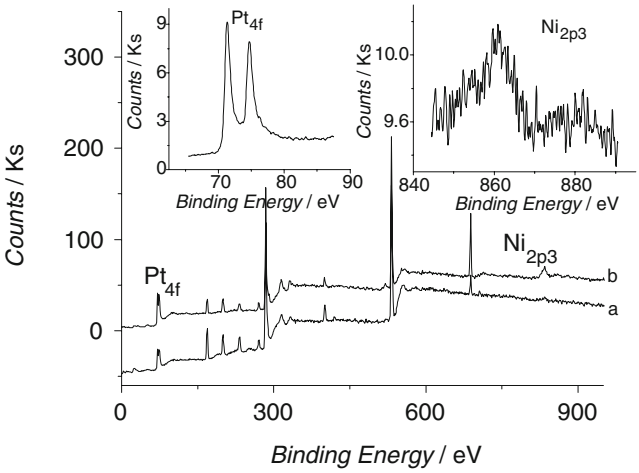

Fig. 5 XPS of Pt–Ni/PAN/MWCNTs obtained by constant potential and CV step (*a*) or direct CV step (*b*). Pt–Ni solution concentration ratio, 1:1

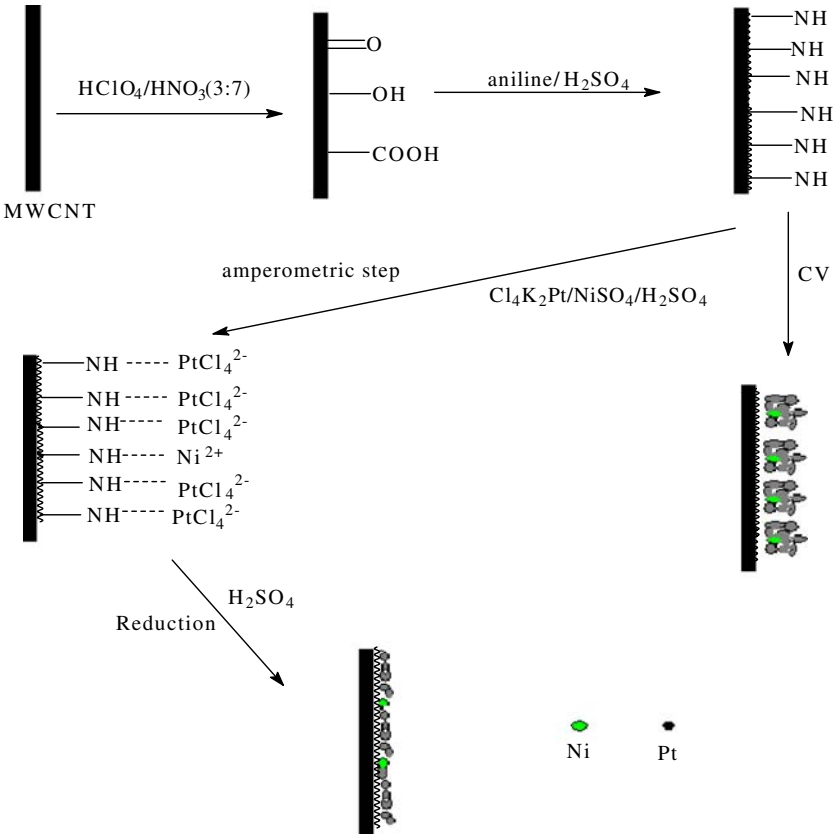

Scheme 1 Synthesized polyaniline coat-MWCNTs film with amidocyanogen

the defects in the linear structure of the polymer [28]. Figure 2b shows the CVs of bare WGE (e), Ni/PAN/MWCNTs/WGE (f), Pt/PAN/MWCNTs/WGE (a), Pt–Ni [solution concentration ratio of Pt–Ni of 1:1 (b), 1:3 (c) and 1:6 (d)]/PAN/MWCNTs/WGE in 0.5 M $HClO_4$. It can be seen that the reversible hydrogen adsorption–desorption peaks between −0.20 and 0.00 V, preoxidation–reduction between 0.40 and 1.44–1.12 V of the Pt surface at Pt/PAN/MWCNTs. An irreversible anodic peak at 0.98 V is relative to the oxidation of Ni^{2+} to Ni^{3+} in curve b to d and in line with a previous work [1]. The current densities associated with the reversible hydrogen adsorption region are obviously decreasing due to the decrease of Pt activated sites [1]. Actually, the platinum–nickel nanocomposites can also be obtained by directly CV method in 0.1 mM Cl_4K_2Pt–0.1 mM $NiSO_4$–0.1 M H_2SO_4. The CVs are the same to that in Fig. 2. The detailed studies are shown in the following.

Physical characterization and structural studies

Figure 3 shows FE-SEM micrograph of Pt–Ni (solution concentration rate, 1:1)/PAN/MWCNTs using a constant potential at −0.3 V for 400 s and CV step (a) or directly CV (b) step. The different potential (E_a) in the former method was investigated; the nanoparticles can be directly deposited with an accumulative effect in E_a<−0.4 V (not shown). However, a homogeneous dispersion nanocomposites arrays can be seen with a size of 0.05–0.1 μm by a constant potential of −0.3 V then conversion in CV (Fig. 3a). Only a little nanocomposite can be obtained in E_a>−0.3 V then conversion in CV (not shown). The surface morphology shows a lot of islands formed by plentiful of

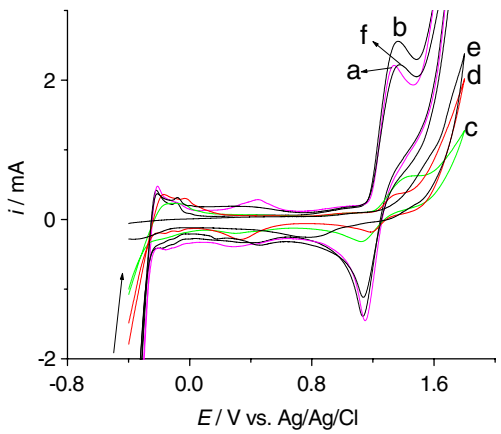

Fig. 6 CVs of 0.1 mM CO at Ni/PAN/MWCNTs/WGE (*e*), Pt–Ni (1:1)/MWCNTs/WGE (*f*), Pt/PAN/MWCNTs/WGE (*a*), Pt–Ni/PAN/MWCNTs/WGE made in solution concentration ratio of Pt:Ni of 1:1 (*b*), 1:3 (*c*), and 1:6 (*d*) using constant potential and CV step. Buffer: 0.5 M $HClO_4$. Scan: 50 mV s^{-1}

Table 1 The redox of 0.1 mM CO at Pt, Ni, and Pt–Ni/PAN/MWCNT/WGE and Pt–Ni/MWCNT/WGE

Sample	Pt/PAN / MWCNTs	Ni/PAN / MWCNTs	Pt-Ni/PAN / MWCNTs (1:1)	Pt-Ni/PAN / MWCNTs (1:3)	Pt-Ni/PAN / MWCNTs (1:6)	Pt-Ni/MWCNTs (1:1)
ΔE_0 (V)	0.227	0.296	0.227	0.297	0.162	0.251
ΔE (V)	0.188	0.315	0.34	0.291	0.158	0.272
[O]-i_{CO}/i_0[a]	1.39	1.31	2.57	1.27	1.25	1.47
[R]-i_{CO}/i_0	1.97	1.16	1.44	1.43	1.25	1.52

[a] The rate of oxidation peak current at about 1.4 V (preoxidation–reduction) before (i_0) and after (i_{CO}) in 0.1 M CO in 0.5 M $HClO_4$.

nanoparticles with sizes of 0.2–1 μm by careful observation using directly CV method (Fig. 3b).

Figure 4 shows the XRD of Pt–Ni (solution concentration ratio, 1:1)/PAN/MWCNTs nanocomposites obtained by constant potential and CV step (a) or directly CV (b) step. All the peaks at different angles (2θ) are from hcp Ni and Pt. The diffraction peaks for Ni (54.4° and 77.5°) are attributable to fcc Ni (200) and (220), and for Pt (39.8° and 46.2°) are matching to fcc Pt (111) and (200). The average grain size of the fcc Ni and Pt particles are calculated to be 8.2 and 10.3 nm in curve (a), 38.5 and 15.4 nm in curve (b) by Scherrer equation, respectively. These document that the Pt–Ni alloy nanocomposites are successfully deposited on PAN/MWCNTs; the size in direct CV is larger than that in the former method; it is in line with the results in FE-SEM micrograph.

Figure 5 shows the XPS of Pt–Ni/PAN/MWCNTs nanocomposites (solution concentration ratio, 1:1) obtained by constant potential and CV (a) or direct CV method (b). The $Pt_{4f7/2}$ and $Pt_{4f5/2}$ peaks respectively appear at 71.4 and 74.1 eV with a theoretical ratio of 4:3 (inset). The peaks for Pt^{2+} and Pt^{4+} at 73.8 and 74.6 eV were not found, indicating that Pt is present in the zero-valent metallic state in PAN/MWCNTs. The $Ni_{2p3/2}$ peaks at 852.6 and 854.0 eV are ascribed to Ni (0), NiO, respectively [1]. From the original date of XPS (not shown), the content for Pt and Ni is 0.71% and 0.04% using method (a); and 1.67% and 0.16% using method (b); hence, the real ratio of the content of Pt and Ni in the Pt–Ni/PAN/MWCNTs nanocomposites is 17:1 in constant potential and CV step and 10:1 in direct CV method. The real ratio of Pt and Ni in the nanocomposites was 8:1 or 7:1 in the solution concentration ratio of Pt and Ni of 1:3 or 1:6 using directly CV method. These illustrate that the Pt is major component in the nanocomposites. This probably explains as follow: the Ni precursor is positively charged, the precursor complex of Pt is negatively charged, and the PAN is likely to be protonated at the pH used for the electrodeposition; thus, the PAN/MWCNTs complex is advantageous for Pt electrodeposition.

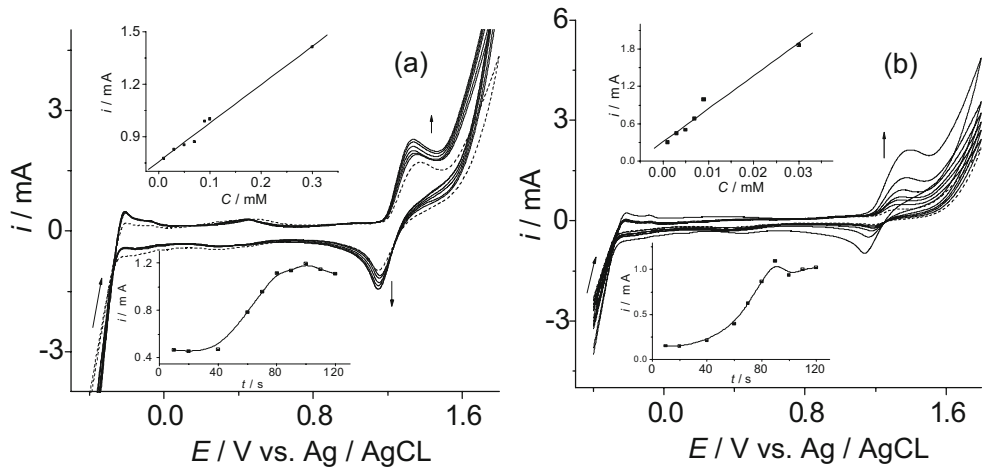

Fig. 7 **a** CVs of CO (0.01, 0.03, 0.05, 0.07, 0.09, 0.3, 0.5, and 0.7 mM) at Pt/PAN/MWCNTs/WGE; *upper inset* the reduction peak currents of CO depend on the concentration. *Lower inset* the accumulation effect of 0.1 mM CO at Pt/PAN/MWCNTs/WGE. **b** CVs of CO (1.0, 3.0, 5.0, 7.0, 9.0, 30.0, and 50.0 μm) at Pt–Ni/PAN/MWCNTs/WGE made in solution concentration ratio of Pt–Ni of 1:1 using constant potential and CV step; *upper inset* the oxidation peak currents of CO depend on the concentration. *Lower inset* the accumulation effect of 0.1 mM CO at Pt–Ni/PAN/MWCNTs/WGE. Buffer: 0.5 M $HClO_4$. Scan: 50 mV s^{-1}

Based on above facts, Scheme 1 can be suggested in the following: the polyaniline coat-MWCNTs film with amidocyanogen was electrosynthesized; then, the complex of –NH–$PtCl_4^{2-}$ and –NH–Ni^{2+} was obtained in constant potential to form the Pt–Ni alloy nanocomposites. Actually, the alloy nanocomposites can also be directly electrodeposited at the film with an accumulative effect.

The redox of CO at Pt–Ni/PAN/MWCNT/WGE

Figure 6 shows the CVs of 0.1 mM CO at Ni/PAN/MWCNTs/WGE (e), Pt–N(1:1)/MWCNTs/WGE (f), Pt/PAN/MWCNTs/WGE (a), Pt–Ni/PAN/MWCNTs/WGE made in the solution concentration ratio of Pt–Ni of 1:1 (b), 1:3 (c) and 1:6 (d) (using constant potential and CV step) in 0.5 M $HClO_4$. The redox parameters were summarized in Table 1. All the electrodes show an electrocatalysis towards CO redox with increased response. PAN/MWCNTs/WGE only gave a small reduction peak at about 0.8 V (no CV shown); a little increase can be seen at Ni/PAN/MWCNT/WGE. However, Pt/PAN/MWCNTs/WGE and Pt–Ni (1:1)/PAN/MWCNTs/WGE respectively show an excellent electrocatalysis toward the reduction or oxidation of CO. The effect is decreasing with the successive increase of Ni. The reason is contributed to that little neighboring Ni can remove the reaction intermediates more quantity neighboring Ni could result in the decrease of Pt activity sites. Therefore, the Pt and Pt–Ni (made in the solution concentration ratio of Pt–Ni of 1:1)/PAN/MWCNTs/WGE can be selected for CO electroanalysis.

The accumulation effect of Pt or Pt–Ni (made in the solution concentration ratio of Pt–Ni of 1:1)/PAN/MWCNTs/WGE toward the redox of 0.1 mM CO was investigated; the results are shown in insets in Fig. 7. It can be seen that the oxidation or reduction response of CO reaches the largest at Pt or Pt–Ni/PAN/MWCNTs/WGE in 90 s, respectively. The reduction peak currents of CO at Pt/PAN/MWCNT shows linearity in a concentration range of 0.01–0.7 mM (i(A)=7.55×10^{-4}+2.21 C (M), R=0.994; LOD=5.0 μM, 3σ; SOD (standard deviation), 2.9%, n=5.); the oxidation peak currents of CO at Pt–Ni/PAN/MWCNTs/WGE show linearity in a concentration range of 1.0–50 μm (i(A)=3.16×10^{-4}+53.11 C (M), R=0.983, LOD=0.5 μM, 3σ; SOD, 4.3%, n=5.). In comparison with the reported results using only MWCNTs electrode (LOD=0.60 μg ml^{-1}=21.4 μM) [21] or only Pt electrode (LOD=1.7 ppm) [27, 29], this work shows a lower detection limit.

Conclusion

This work suggests a new route of Pt–Ni alloy nanocomposites on polyaniline-MWCNTs by electrochemical method. The study has proved that little neighboring Ni can remove the reaction intermediates and more quantity neighboring Ni can result in the decrease of activity sites. The nanocomposites were successfully used as electroanalysis for CO. The Pt–Ni (real ratio17:1)/PAN/MWCNTs shows an excellent electrocatalysis towards CO oxidation. Further studies are focused on deposition mechanism, electrocatalytic efficiency, and practical application in the electroanalysis of CO and fuel cells.

Acknowledgements The authors gratefully acknowledge financial support from Natural Science Foundation of Anhui Province of China (No. 070415210), Science and Technology Program Foundation of Hefei City (No. 20071032), and Doctor Foundation of Hefei University of Technology (2005).

References

1. Zhao Y, Ea YF, Fan LZ, Qiu YF, Yang SH (2007) Electrochim Acta 52:5873, doi:10.1016/j.electacta.2007.03.020
2. Sathe BR, Risbud MS, Patil S, Ajayakumar KS, Naik RC, Mulla IS et al (2007) Sens Actuators A 138:376, doi:10.1016/j.sna.2007.05.013
3. Otagawa T, Madou M, Wing S, Rich-Alexander J (1990) Sens Actuators B 1:319, doi:10.1016/0925-4005(90)80223-M
4. Durrani SMA, Al-Kuhaili MF (2008) Mater Chem Phys 109:56
5. Mulrooney J, Clifford J, Fitzpatrick C, Chambers P, Lewis E (2008) Sens Actuators A 144:3
6. Zhuiykov S (2008) Sens Actuators B 129:431, doi:10.1016/j.snb.2007.08.046
7. Wu RJ, Hu CH, Ye CT, Su PG (2003) Sens Actuators B 96:596, doi:10.1016/S0925-4005(03)00646-4
8. Chen CL, He JB, Xu D, Tan XL, Zhou X, Wang XK (2005) Sens Actuators B 107:866, doi:10.1016/j.snb.2004.12.037
9. Azevedo DC, Pinheiro ALN, Torresi RM, Gonzalez ER (2002) J Electroanal Chem 532:43, doi:10.1016/S0022-0728(02)00912-9
10. Bujno K, Bilewicz R, Siegfried L, Kaden T (1996) J Electroanal Chem 407:131, doi:10.1016/0022-0728(95)04501-5
11. Mathiyarasu J, Remona AM, Mani A, Phani KLN, Yegnaraman V (2004) JSS Electrochem 8:968, doi:10.1007/s10008-004-0526-9
12. Neyerlin KC, Singh A, Chu D (2008) J Power Sources 176:112, doi:10.1016/j.jpowsour.2007.10.030
13. Murthi VS, Urian RC, Mukerjee S (2004) J Phys Chem B 108:11011, doi:10.1021/jp048985k
14. Anderson AB, Roques J, Mukerjee S, Murthi VS, Markovic NM, Stamenkovic V (2005) J Phys Chem B 109:1198, doi:10.1021/jp047468z
15. Colón-Mercado HR, Kim H, Popov BN (2004) Electrochem Commun 6:795, doi:10.1016/j.elecom.2004.05.028
16. Yen CH, Shimizu K, Lin YY, Bailey F, Cheng IF, Wai CM (2007) Energy Fuels 21:2268, doi:10.1021/ef0606409
17. Toda T, Igarashi H, Uchida H, Watanabe M (1999) J Electrochem Soc 146:3750, doi:10.1149/1.1392544
18. Ueda T, Katsuki S, Takahashi K, Narges HA, Ikegami T, Mitsugi F (2008) Diam Relat Mater in press
19. Espinosa EH, Ionescu R, Chambonb B, Bedis G, Sotter E, Bittencourt C et al (2007) Sens Actuators B 127:137, doi:10.1016/j.snb.2007.07.108

20. Zhang B, Fu RW, Zhang MQ, Dong XM, Lana PL, Qiu JS (2005) Sens Actuators B 109:323, doi:10.1016/j.snb.2004.12.066
21. He JB, Chen CL, Liu JH (2004) Sens Actuators B 99:1, doi:10.1016/j.snb.2003.12.068
22. Burghard M (2005) Surf Sci Rep 58:1
23. Jin GP, Ding YF, Zheng PP (2007) J Power Sources 166:80, doi:10.1016/j.jpowsour.2006.12.087
24. Tian ZQ, Jiang SP, Liang YM, Shen PK (2006) J Phys Chem B 110:5343, doi:10.1021/jp056401o
25. Villers D, Sun SH, Serventi AM, Dodelet JP, Desilets S (2006) J Phys Chem B 110:25916, doi:10.1021/jp065923g
26. Wildgoose GG, Banks CE, Compton RG (2006) Small 2(2):182, doi:10.1002/smll.200500324
27. Knake R, Jacquinot P, Hodgson AWE, Hauser PC (2005) Anal Chim Acta 549:1, doi:10.1016/j.aca.2005.06.007
28. Zhang L, Lian JY (2007) J Electroanal Chem 611:51, doi:10.1016/j.jelechem.2007.08.002
29. Xing XK, Liu CC (1991) Electroanalysis 3:111, doi:10.1002/elan.1140030207